Soldagem & Inspeção. 2016;21(2):146-155
http://dx.doi.org/10.1590/0104-9224/SI2102.04

Microstructural Development in a TRIP-780 Steel Joined by Friction Stir Welding (FSW): Quantitative Evaluations and Comparisons with EBSD Predictions

Gladys Perez Medina[1], Hugo Lopez Ferreira[2], Patricia Zambrano Robledo[3], Argelia Miranda Pérez[1], Felipe A. Reyes Valdés[1]

[1] Corporación Mexicana de Investigación en Materiales, Postgraduate Studies, Saltillo, Coah. México.
[2] University of Wisconsin-Milwaukee, Materials Department, Milwaukee, WI, USA.
[3] Universidad Autónoma de Nuevo León, FIME, Aeronautical Engineering, NL, México.

Received: 23 Jan., 2016
Accepted: 30 Mar., 2016

E-mail: gladysperez@comimsa.com (GPM)

Abstract: The present work describes the effect of FSW on the result microstructure in the stir zone (SZ), thermo-mechanically affected zone (TMAZ), heat affected zone (HAZ) and base metal (BM) of a TRIP-780 steel. X-ray diffraction (XRD), optical microscopy (OM) and EBSD were used for determinations retained austenite (RA) in the SZ, It was found that the amount of RA developed in SZ was relatively large, (approximately 11% to 15%). In addition, recrystallization and the formation of a grain texture were resolved using EBSD. During FSW, the SZ experienced severe plastic deformation which lead to an increase in the temperature and consequently grain recrystallization. Moreover, it was found that the recrystallized grain structure and relatively high martensite levels developed in the SZ lead to a significant drop in the mechanical properties of the steel. In addition, microhardness profiles of the welded regions indicated that the hardness in both the SZ and TMAZ were relatively elevated confirming the development of martensite in these regions. In particular, to evaluate the mechanical strength of the weld, lap shear tensile test was conducted; exhibited the fracture zone in the SZ with shear fracture with uniformly distributed elongation shear dimples.

Key-words: AHSS; TRIP steel; XRD; EBSD; FSW.

Microstructural Desenvolvimento em um Aço TRIP-780 Unido por Soldagem por Atrito com Pino Não Consumível (FSW): Comparações e Avaliações Quantitativas com EBSD Predições

Resumo: O presente trabalho descreve o efeito do processamento FSW na microestrutura resultante na zona soldada, zona termomecanicamente afetada (TMAZ), zona afetada pelo calor (ZAC) e no metal base (MB) de um aço TRIP-780. Difração de raios-X (DRX), microscopia óptica (MO) e EBSD foram utilizados para a determinação de austenita retida (RA) na SZ. Verificou-se que a quantidade de RA desenvolvida na SZ foi relativamente grande, (cerca de 11% a 15%). Além disso, a recristalização e a formação de textura de grão foram resolvidas usando EBSD. Durante friction stir welding, FSW (Soldagem por Atrito com Pino Não-consumível), a SZ experimentou severa deformação plástica que conduziu a um aumento na temperatura e, consequentemente, recristalização dos grãos. Verificou-se que a estrutura do grão recristalizado e níveis relativamente elevados de martensita desenvolvidos na SZ, conduziram a uma redução significativa nas propriedades mecânicas do aço. Além disso, os perfis de microdureza das regiões soldadas indicam que a dureza, tanto na SZ como na TMAZ foi elevada, confirmando o desenvolvimento de martensita nestas regiões. Em particular, foi visualidade na zona fundida trincas alongadas em perfil y, distribuída uniformetente.

Palavras-chave: AHSS; Aço TRIP; XRD; EBSD; FSW.

1. Introduction

Advanced high strength steels (AHSS) display complex multi-phase microstructures and unique combinations of high strength and ductility for applications in the automotive sector. Typical AHSS microstructures consist of mixtures of bainite (B), ferrite (F), martensite (M), and retained austenite (RA) [1]. In recent years these steels have been the subject of extensive work due to their relatively high toughness [2,3]. When AHSS are joined by friction stir welding (FSW), a precise characterization of the welded microstructures is of great importance as they account for the weld toughness [4]. In FSW exceptionally large temperature gradients coupled with elevated plastic strains and strain rates leads to the

development of recrystalized microstructures containing various amounts of B, F, M and RA [5-7]. In particular, the presence of retained austenite and the austenite-to-martensite transformation during FSW can adversely affect the steel toughness [8].

Among the AHSS, transformation induced plasticity (TRIP) steels have been developed which contain relatively large amounts of RA. The exhibited volume fractions of RA are strongly influenced by the previous thermal mechanical history, as well as the steel composition, particularly Mn, Nb and Si contents. In general, high amounts of RA (of the order of 15%) are desirable in TRIP steels for applications that require high toughness such as a sudden vehicle crash [1,9]. Under these conditions, RA transforms to martensite under the effect of high strain rate plastic deformation [10-12]. Various characterization techniques have been employed for determinations of RA in these steels including X-ray diffraction and color metallography [13,14]. Nevertheless, there is limited work on the characterization and quantification of the phases developed in the different regions of TRIP steels joined by FSW. In steels joined by FSW, at least three regions have been identified to be developed; the stir zone (SZ), the thermo-mechanically affected zone (TMAZ) and the heat affected zone (HAZ).

Among the published works, Lomholt et al. [15] investigated the weldability of a TRIP steel joined by FSW. In their work, they included electron backscattering diffraction (EBSD) besides the conventionally used characterization techniques. However, no effort was made in making quantitative determinations of the developed phases. More recently, Miranov et al. [16] demonstrated that EBSD is an important tool for the characterization of microstructural features including texture control in materials welded by FSW. From these works, it is obvious that EBSD can provide fundamental insight into the microstructural evolution as well as for microstructural quantification [7].

Accordingly, in this work various analytical techniques for microstructural resolution were considered and compared with EBSD estimations of the various phases developed in a TRIP 780 steel joined using FSW. In particular, the exhibited volume fractions of RA and M in the various welded regions (BM, SZ and HAZ) were quantified in order to disclose possible phase transformation reactions.

2. Experimental Procedure

2.1. Microstructural characterization

The investigated TRIP 780 steel was supplied in the form of 2.7 mm thick sheet. Table 1 gives the chemical composition of the TRIP 780 steel whereas Table 2 gives the exhibited mechanical properties. In addition, microstructural characterization and phase quantification were carried out by optical microscopy (OM) using an Image-Pro Plus analyzer, X-ray diffraction (XRD) in a Phillips PW 3040/00 X'Pert MPD with Cu Kα radiation and scanning electron microscopy in a Phillips XL-30 equipped with electron back scattering diffraction (EBSD) EDAX/TSL. The acceleration voltage employed was 20kV and the working distance 80 × 70 µm with a step size of 0.35 µm. The etchings solutions used were Klemm's I (1 g $K_2S_2O_5$ potassium metabisulfite, 79.4 g $Na_2S_2O_3$-$5H_2O$ Sodium Thiosulfate) to reveal the structure of the HAZ, TMAZ and SZ. Lepera (1% aqueous sodium metabisulfite with 4% Picral) was used to reveal the microstructure of the base metal (BM) and 2% Nital followed by heat tinting, to reveal the ferrite grain boundaries. To evaluate the mechanical strength of the weld, lap shear tensile tests of the cross section of the weld was conducted using a fully computerized united tensile testing machine at a crosshead dis- placement speed of 10 mm/min in air at room temperature (Std. ASTM E08 sub-size).

Table 1. Chemical composition of the AHSS TRIP 780.

Wt% TRIP 780	C	S	Mn	P	Si	Cr	Ni	Mo	Cu	V	Nb	Ti
	0.1	<0.002	1.98	<0.002	2.35	<0.06	<0.04	<0.03	0.012	0.019	<0.004	0.01

Table 2. Mechanical properties of the AHSS TRIP 780.

Base Metal	Yield Strength [MPa]	Ultimate Tensile Strength [MPa]	Elongation [%]	Hardness [HV]
TRIP 780	652	854	20	254

2.2. Friction stir welding processing

The welding conditions in the FSW process were a welding speed and heat input of 200 mm/min and 5592 J/mm respectively. Plunge in speed of 2.4 mm/min and rotational speed of 800 Rev. / min. The specimens of the size of 244 mm length × 70 mm width were machined from TRIP780 steels (Figure 1a). The lap joint was made using the CNC machine Bridgerport VMC 760XP3. The equipment could achieve maximum spindle speeds of up to 12000 RPM and a maximum spindle power of 18.5 kW or 25 hp. The tool used in this work was made of Poly Crystalline Boron Nitride (PCBN) and it was fabricated by MegaStir Technologies with a cylindrical tool profile. It comprises of 36 mm shoulder diameter, 7 mm pin diameter and 4mm pin length.

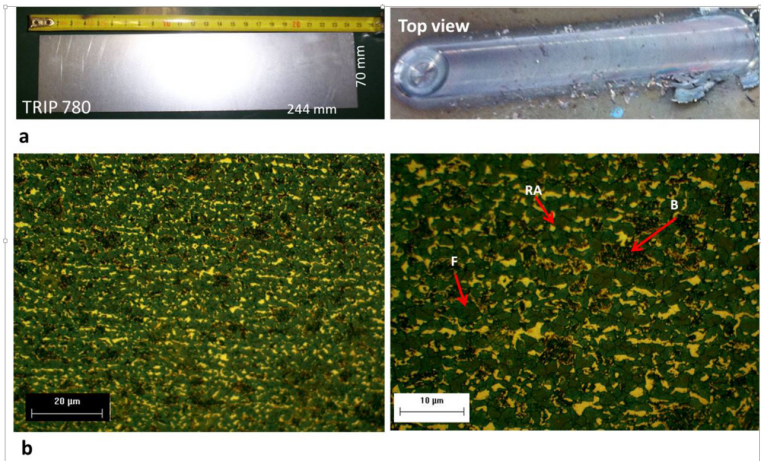

Figure 1. (a) Top view of FSW and dimensions; (b) Optical micrograph of the AHSS TRIP780 in the BM. Etchant: Picral.

3. Results and Discussion

3.1. Welded microstructures

Metallographic determinations closely followed the published methods for identification and characterization of phases in TRIP steels [13,17], the etching applied in the as-received TRIP780 steel was 4% picral (4 g dry picric acid in 100 mL ethanol), mixed with a few drops of concentrated hydrochloric acid (1 mL per 100 mL of picral solution) and 10% aqueous sodium metabisulfite solution (1 gr sodium metabisulfite with 100 mL of water). The purpose of the hydrochloric acid was to improve grain boundary etching and to sharpen the appearance of any iron carbides. The steel cross-section was mounted in bakelite and after polishing the sample was first dipped in the picral solution for 18 to 20 seconds. During the whole etching process, the specimen was gently oscillated. After etching in picral, the sample was immediately washed with water followed by ethanol, and then dried in hot air. Picral was chosen over Nital because of its effect on a better delineation of carbides and bainite. Nital attacks ferrite grains and grain boundaries, but picral preferentially attacks the ferrite and carbide interfaces. Once the microstructural observations were completed after the first stage of etching, the sample was further dipped in a freshly prepared solution of sodium metabisulfite for six to eight seconds, and then immediately washed in water followed by ethanol, and then dried in hot air.

The exhibited microstructural features of the TRIP steel are shown in Figure 1b. Notice the presence of a mixture of ferrite and bainite including retained austenite that appears as small bright white particles preferentially located between bainite layers. The presence of RA at bainite interphase boundaries agrees with the transmission electron microscopy observations of Chen et al. [18] of RA at these locations. The color micrograph of Figure 1 also reveals that ferrite can be clearly distinguished from bainite (green = ferrite, dark brown = bainite). The resultant microstructures found in the HAZ, TMAZ and SZ using OM are shown in Figures 2a-c, respectively. Notice that the color tinting of the resultant phases consists of dark brown for M, blue for B, green for F and small bright white particles for RA.

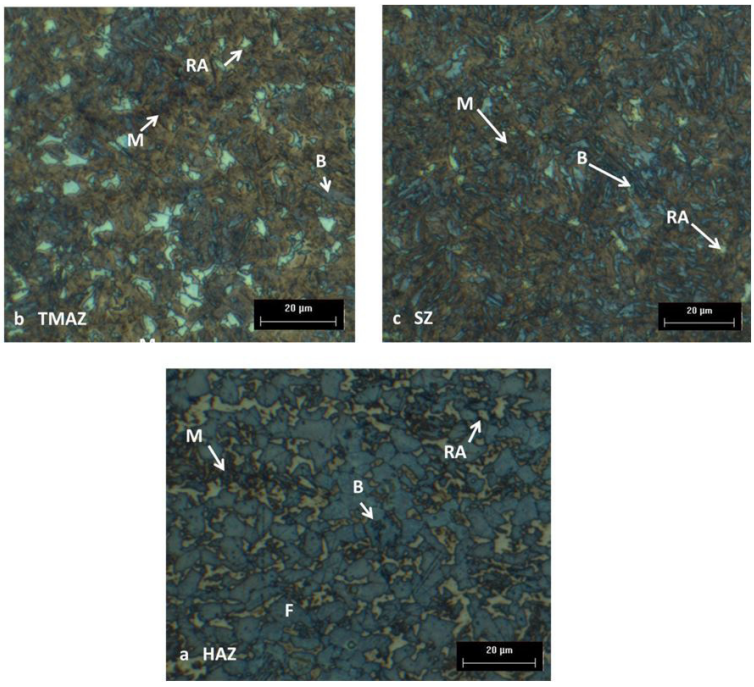

Figure 2. Optical micrograph of (a) HAZ; (b) TMAZ; and (c) SZ. Etchant: Klemm's I.

Figure 3 gives an overview of the different microstructures developed in the various weld zones produced by FSW. As for the expected morphological changes in the various weld regions, next to the welded region is the HAZ. This region can be heated sufficiently to induce some structural modifications with no changes in the grain structure. The alteration of properties in the HAZ may include some changes in strength and ductility [19,20] but the steel is expected to keep essentially the same properties as those of the BM.

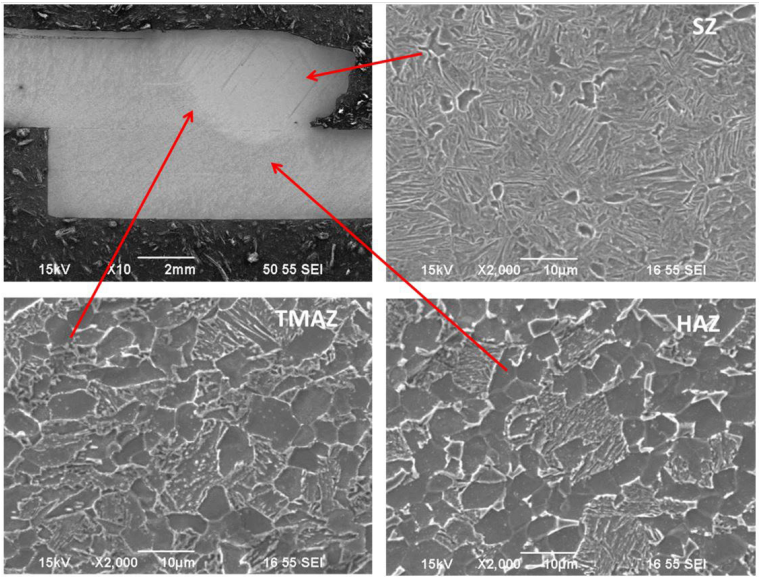

Figure 3. SEM images of the microstructure in the three zones of FSW.

The TMAZ encompasses all of the plastically deformed material within the joint region. In this region, the workpiece is sufficiently heated and grain structure heavily deformed to induce grain recrystallization [20,21]. In addition, a fully recrystallized structure develops in the SZ as this region is under the effect of severe compression loading at elevated temperatures. The phases developed in the final recrystallized grain structure are expected to strongly depend on the peak temperatures reached in the work piece [22], as well as the actual cooling rates and steel composition.

3.2. Phase quantification

Quantitative determinations of the various phases in the BM, SZ and HAZ are given in Figure 4. Notice from this figure that there is not a significant variation in the exhibited amounts of B and F in the HAZ when compared with the BM. In particular, the amounts of ferrite and bainite decrease, in the case of ferrite in the HAZ (38%) and in the SZ (33%). In contrast, there is a slight increase in the amount of RA and M. In the case of RA the vol. % present in the different weld zones was determined by both, image analysis (Figure 4a) and by XRD (Figures 4b-d) through the use of Cu Kα radiation. An estimation of the amount of retained austenite was made by considering the following Equation 1 [14]:

$$V\gamma = \frac{1.4I_\gamma}{I_\alpha + 1.4I_\gamma} \quad (1)$$

where Iγ is the average intensity of the austenite peaks and Iα is the highest intensity of the ferrite peak. The XRD results and the applied parameters are given in Table 3. Notice in particular, that the vol. % RA in the HAZ and in the SZ goes up to 15% compared with 11% in the BM. Apparently, the amount RA after the high temperature incursion increased in both the SZ and HAZ regions.

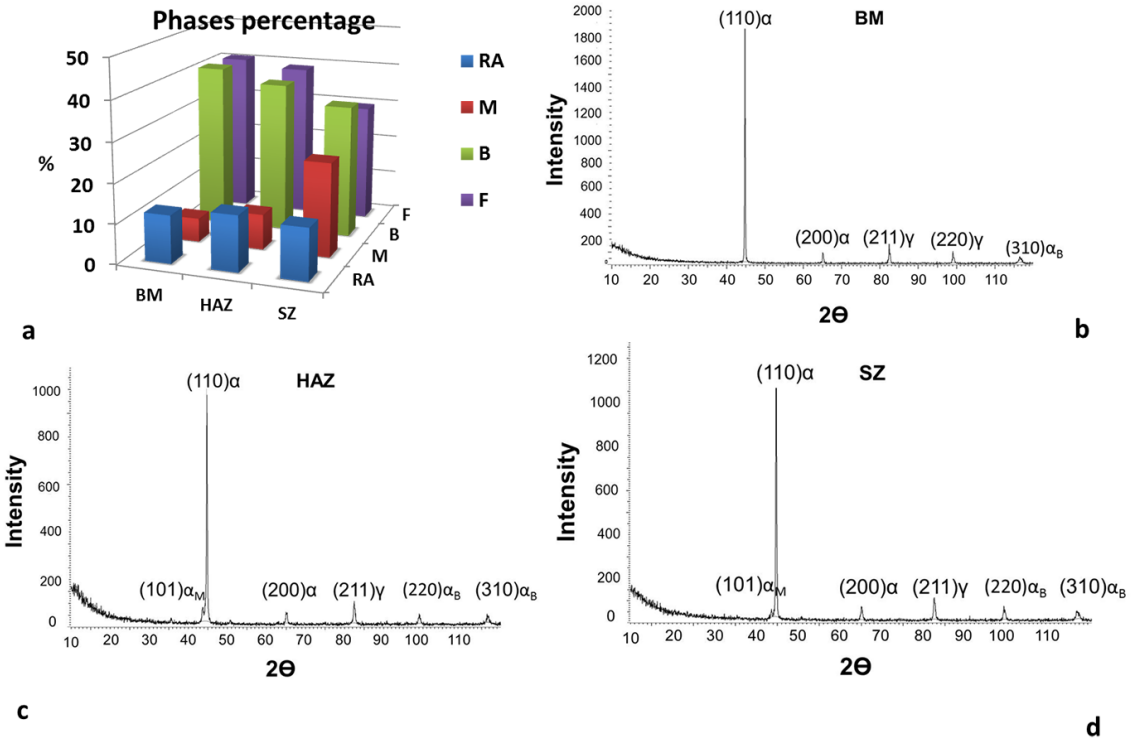

Figure 4. (a) Percent phases in the BM, HAZ, and SZ of FSW TRIP780 steel and X-ray diffraction peaks corresponding to the (b) BM, (c) HAZ and (d) SZ.

Table 3. XRD results and parameters applied for FSW processes in a TRIP780 steel.

Sample	Intensity (I)			RA (%)
	α-Iron	γ-Iron		
BM	(110)-1825	(211)-200	(220)-150	11.83
SZ	(110)-1000	(211)-130	-	15.39
HAZ	(110)-1125	(211)-145	-	15.28

From Figure 4, apparently, there is an increase in the vol. % of precipitated martensite particularly in the SZ. Notice that the amount of precipitated martensite increases up to 8.96% in the HAZ and as high as 23.72% in the SZ. Apparently, the SZ reaches peak temperatures of or above A3 (1147K) which upon cooling [23], the cooling rates are high enough to promote the martensite transformation. Hence, it is expected that the exhibited weld microstructures are a result of a combination of the implemented processing factors. The dominant factors can be defined as the steel composition (preferentially C, Mn and Si) and the state of mechanical and the thermal cycles experienced in the various weld regions [22,24].

EBSD is a useful tool for determinations of grain evolution and texture development in steels exposed to severe thermal mechanical processing such in the SZ during FSW [25]. The experimental outcome using EBSD in the FSW process on the grain structure modifications can be described by (a) the initial grain structure is first reoriented into a flow pattern around the tool due to the geometrical requirements associated with the applied strain (see Figure 5). (b) Simultaneously, the original grains are split into regular arrays of nearly parallel bands. In turn, this indicates the beginning of a grain subdivision process in the deformed grain structure. (c) As the applied plastic strain increases, the band boundary increases in the regions exposed to the pin of the tool (SZ). (d) Eventually, this leads to the formation of a lamellar-type microstructure [16,25]. Figure 6 shows a microstructure map with the display of boundaries and orientation relationships (OR) between austenite and ferrite grains.

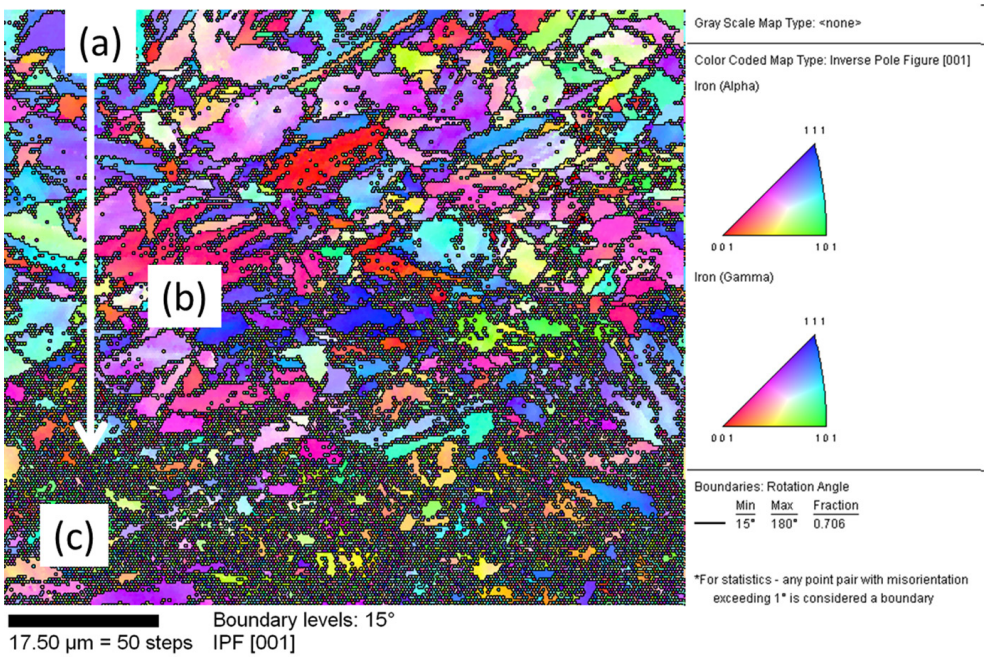

Figure 5. EBSD map from directly ahead of the tool, showing the effect of the progressively increasing strain and temperature with proximity to the tool (a). Moving from top to bottom of the map, grains can be seen splitting into deformation bands, which increase in misorientation and reduce in spacing, parallel new high-angle grain boundaries that then break-up along their length by thermally assisted boundary migration to form fine grains in the SZ (b). The material immediately next to the pin surface is shown in (c).

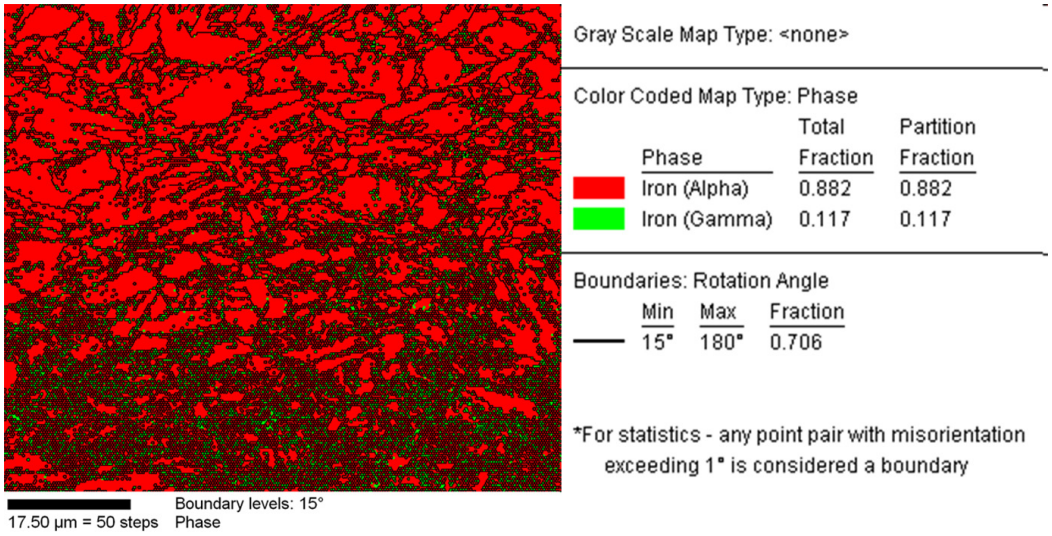

Figure 6. Phase distribution obtained with the Kam-threshold method displayed on the same microstructure that shown Figure 5. They are characteristic for boundaries that are responsible for α-γ phase transformation.

The relative amounts of RA and F can be easily distinguished by EBSD since they have different crystallographic structures [26]. Martensite is either not indexed by the software or it is shown as an area with low pattern quality (PQ) and a high density of particular grain boundaries. However, bainitic ferrite and ferrite in the present steel have both the same crystallographic structure, bcc, and need further work to be able to be distinguished. In this work, a quantification of the amount of RA in the SZ carried out by considering an area of approximately 80 µm x 70 µm for EBSD, in the case of XRD diffraction the section exanimated was of 2mm^2 and finally the sample of the optical microscopy was 80 µm^2. The results of these determinations are plotted in Figure 7 and compared with the ones found by OM and XRD. Considering that the determinations by EBSD are confined to a relatively small area, the amounts of RA (11%) are in good agreement with those obtained by OM (13%) and XRD (15%). Nevertheless, a direct comparison of the amount of RA measured by these methods should be carried out with care keeping in mind the sample size effect. XRD gives quantitative average estimations of RA in a volume which is significantly larger than the EBSD scan area. In addition, the crystal orientation mapping yields similar values but on a local scale which is highly dependent on magnification and on the spatial resolution of the microscope.

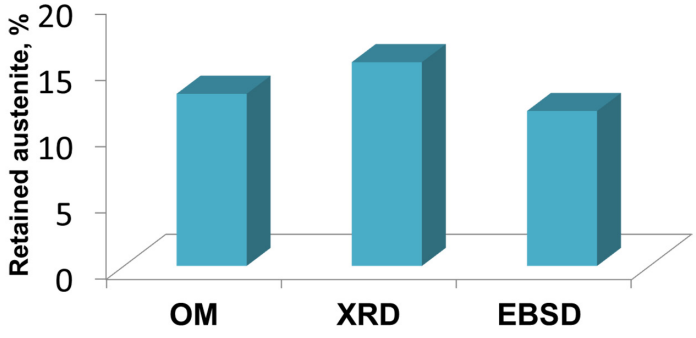

Figure 7. Quantification of retained austenite fraction by different characterization technique.

3.3. Microhardness

Microhardness profiles of the welded regions confirm that relatively high amounts of martensite developed in the SZ. Notice the relatively elevated hardness (near 420 Hv, Figure 8) and the top hat shape of the graph, indicating a significant development of martensite in this region. Apparently, a recrystallized fine γ-grain microstructure formed by the intense plastic deformation imposed on the SZ, yielded upon cooling relatively high amounts of martensite (23%). To some extent, this effect was also experienced in the transition region (Figure 8). Among other factors, the exhibited martensite hardness is strongly dependent on the carbon content and it can reach values of up to 540 VH [9,27]. Carbon build-up in the austenite phase is always likely as in the intercritical region α-Fe precipitation is accompanied by carbon rejection into the surrounding austenite. In the HAZ, the amounts of RA and M were slighty above the ones corresponding to the BM, but the overall hardness was not affected.

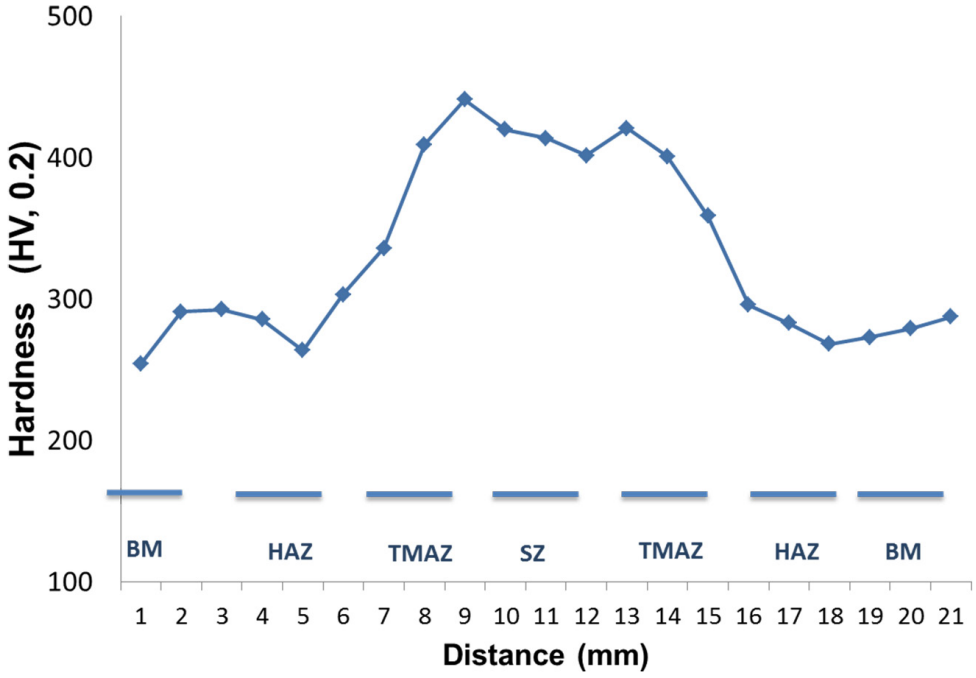

Figure 8. Microhardness profile.

3.4. Lap shear tensile test

The shear tension strength of the welded joints including the BM were evaluated using a lap-shear tensile test (see Figure 9a). From the experimental outcome, it was found that ultimate tensile strength (UTS) of the TRIP780 steel was 854 MPa. In contrast, the maximum UTS values found in the friction stir welded steel were of the order of 316 MPa. Hence, it is evident that friction stir welding of the TRIP780 steel for the parameters and application considered in this work, lead to a reduction in the toughness and ductility. Confirmation for the loss of toughness was found through SEM examinations of the fracture surfaces (see Figure 9b). Figure 9c shows the appearance of the fracture surfaces. It was found that the fracture occurred in the SZ where lap shear markings are developed, as well as uniformly distributed elongated shear dimples [28]. Apparently, FSW lead to a severe deformation of the austenite and subsequent recrystallization, raised the Ms temperature and enhanced the transformation of metastable austenite into martensite as discussed by Patel and Cohen [29]. In their work they suggest that applied tensile is capable of algebraically decreasing the driving force required for the martensitic transformation.

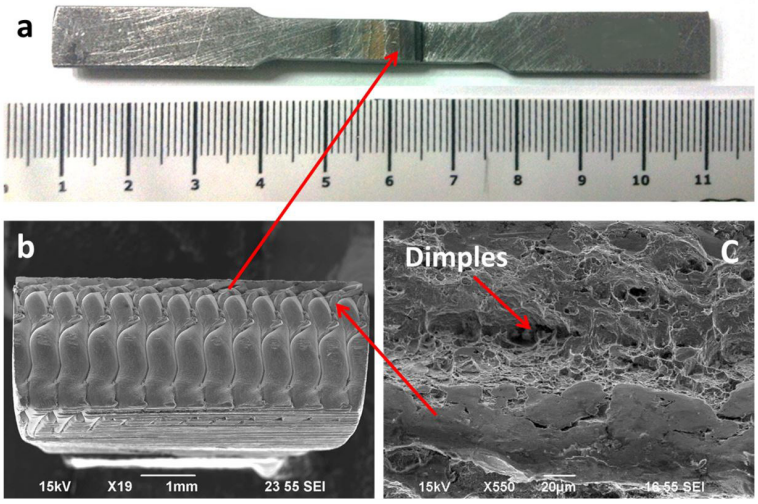

Figure 9. (a) Lap-shear tensile test specimen used to characterize the fracture of TRIP 780 steel; (b) Overall view of the fracture surfaces; (c) fracture appearance with uniformly distributed elongation shear dimples.

4. Conclusions

The weldability of a thin (2.7 mm) sheet of a TRIP 780 steel using FSW has been investigated using color etching, as well as XRD, EBSD and lap shear tensile testing. Color etching enabled the identification of retained austenite, ferrite, bainite and martensite in the SZ, TMAZ, HAZ and BM. In turn, quantitative determinations of the relative amounts of these phases were possible. XRD was also used to confirm the amounts of retained austenite in the SZ. In addition, the EBSD technique was employed for determinations of RA. The quantity of fraction of RA measured by EBSD was somewhat below the ones obtained OM and XRD. This is likely to be due to the sample size effect and the magnifications used. Nevertheless, EBSD is a highly effective tool for determinations of the grain structure and resultant textures in the SZ. In particular, it is found that in the SZ relatively elevated amounts of martensite are formed (above 23%) probably as a result of rapid cooling of a highly strained austenite phase and a recrystallized grain structure. The mechanical properties of the TRIP 780 steel indicates that the SZ region undergoes a somewhat brittle fracture as the lap shear tensile strength drops to values of 316 MPa, which are below those corresponding to the BM (854 MPa).

References

[1] Zhang M, Zhu F, Zheng D. Mechanical properties and retained austenite transformation mechanism of TRIP-Aided steel polygonal ferrite matrix seamless steel tube. Journal of Iron and Steel Research. 2011;18(8):73-78. http://dx.doi.org/10.1016/S1006-706X(11)60107-6.

[2] Shan TK, Li SH, Zhang WG, Xu ZG. Prediction of martensitic transformation and deformation behavior in the TRIP steel sheet forming. Materials & Design. 2008;29(9):1810-1816. http://dx.doi.org/10.1016/j.matdes.2008.03.023.

[3] Miguel V, Martínez A, Coello J, Avellaneda FJ, Calatayud A. A new approach for evaluating sheet metal forming base on sheet drawing test: application to TRIP 700 steel. Journal of Materials Processing Technology. 2013;213(10):1703-1710. http://dx.doi.org/10.1016/j.jmatprotec.2013.04.010.

[4] Cho H-H, Kang SH, Kim S-H, Oh KH, Kim HJ, Chang W-S, et al. Microstructural evolution in friction stir welding of high-strength linepipe steel. Materials & Design. 2012;34:258-267. http://dx.doi.org/10.1016/j.matdes.2011.08.010.

[5] Mishra RS, Mahoney MW, McFadden SX, Mara NA, Mukherjee AK. High strain rate superplasticity in a friction stir processed 7075 Al alloy. Scripta Materialia. 2000;42(2):163-168. http://dx.doi.org/10.1016/S1359-6462(99)00329-2.

[6] Lohwasser D, Chen Z. Friction stir welding: from basics to applications. Oxford: Woodhead Publishing in Materials; 2010.

[7] Venkateswarlu G, Singh AK, Davidson J, Tagore GR. Effect of microstructure and texture on forming limits in friction stir processed AZ31B Mg alloy. Journal of Materials Research and Technology. 2013;2(2):135-140. http://dx.doi.org/10.1016/j.jmrt.2013.01.003.

[8] Curtze S. Characterization of the dynamic behavior and microstructural evolution of High Strength Sheet Steel. Tampere: Tampere University of Technology; 2009. Publication 833.

[9] Ghosh M, Kumar K, Mishra RS. Friction stir lap welded advanced high strength steel: microstructure and mechanical properties. Materials Science and Engineering. 2011;528(28):8111-8119. http://dx.doi.org/10.1016/j.msea.2011.06.087.

[10] Zackay VF, Parker ER, Fahr D, Busch R. Stability and mechanical properties of some metastable austenitic steels. *Metallurgical and Materials Transactions B, ASM*. 1967;60:253-259.

[11] Banerjee BR, Capenos JM, Hauser JJ. Application of fracture toughness parameters to structural metals. New York: Gordon and Breach Science Publishers; 1966. p. 373-406.

[12] Hanzaki AZ, Hodgson PD, Yue S. Retained austenite characteristic in thermomechanically processed Si-Mn transformation-induced plasticity steels. Metallurgical and Materials Transactions. A, Physical Metallurgy and Materials Science. 1997;28(11):2405-2415. http://dx.doi.org/10.1007/s11661-997-0197-0.

[13] Amar K, Speer JG, Matlock DK. Color tint-etching for multiphase steels. Advanced Materials & Processes. 2003;161(2):27-30.

[14] Meyer M, Cooman DBCD. The influence of Al on the properties of cold rolled C-Mn-Si TRIP steels. In: 41st MWSP Conference Proceedings. Chicago: Iron and Steel Society AIME; 1999. p. 265-276. (vol. 37).

[15] Lomholt TC, Pantleon K, Somers MAJ. Microstructure evolution during friction stir spot welding of TRIP steel. Lyngby: Department of Mechanical Engineering, Technical University of Denmark; 2010.

[16] Miranov S, Sato YS, Kokawa H. Applications of EBSD to microstructural control in friction stir welding. New York: Springer Science; 2009. p. 291-300.

[17] Voort, G. V. Using microstructural analysis to solve practical problems. USA: Buehler; 2004. p. 19-23. (Welding Metallography-Ferrous Metals, vol. 4).

[18] Chen J, Sand K, Xia MS, Ophus C, Mohammadi R, Kuntz ML, et al. Transmission electron microscopy and nanoindentation study of the weld zone microstructure of diode-laser-joined automotive transformation-induced plasticity steel. Metallurgical and Materials Transactions. 2008;39(3):593-603. http://dx.doi.org/10.1007/s11661-007-9389-x.

[19] Lohwasser D, Chen Z. Friction stir welding from basics to applications. Oxford: Woodhead Publishing in Materials; 2010.

[20] Mishra RS, Mahoney MW. Friction stir welding and processing. 2nd ed. Materials Park: ASM International; 2008.

[21] Attallah M. Friction stir welding of aluminum alloys. Germany: Lambert Academic Publishing; 2011.

[22] Matsushita M, Kitani Y, Ikeda R, Ono M, Fujii H, Chung Y-D. Developments of friction stir welding of high strength steel sheet. Science and Technology of Welding and Joining. 2011;16(2):181-188. http://dx.doi.org/10.1179/1362171810Y.0000000026.

[23] Van Dijk NH, Butt A, Zhao L, Sietsma J, Offerman S, Wright J, et al. Thermal stability of retained austenite in TRIP steels studied by synchrotron X-Ray diffraction during cooling. Acta Materialia. 2005;53(20):5439-5447. http://dx.doi.org/10.1016/j.actamat.2005.08.017.

[24] Wei LY, Nelson TW. Correlation of microstructure and process variables in FSW HSLA-65 steel. Welding Journal. 2010;90:95-101.

[25] Mironov S, Sato YS, Kokawa H. Microstructural evolution during friction stir-processing of pure Iron. Acta Materialia. 2008;56(11):2602-2614. http://dx.doi.org/10.1016/j.actamat.2008.01.040.

[26] Zaefferer S, Romano P, Friedel F. EBSD as a tool to identify and quantify bainite and ferrite in low- alloyed Al-TRIP steel. Journal of Microscopy. 2008;230(Pt 3):499-508. http://dx.doi.org/10.1111/j.1365-2818.2008.02010.x. PMid:18503676.

[27] Reed-Hill RE, Abbaschian R. Physical metallurgy principals. 3rd ed. Boston: PWS Kent Publishing Company; 1996. p. 651-660.

[28] ASM International. ASM Handbook: welding, brazing and soldering. Materials Park: ASM; 2003. 755 p. (vol. 6).

[29] Patel JR, Cohen M. Criterion for the action of applied stress in the martensitic transformation. Acta Metallurgica. 1953;1(5):531-538. http://dx.doi.org/10.1016/0001-6160(53)90083-2.